

# Age-related Decline of Visual Working Memory: Behavioral Results Simulated with a Dynamic Neural Field Model

Matthew C. Costello<sup>1</sup> and Aaron T. Buss<sup>2</sup>

## Abstract

■ Visual working memory (VWM) is essential for executive function and is known to be compromised in older adults. Yet, the cognitive and neural processes associated with these age-related changes remain inconclusive. The purpose of this study was to explore such factors with a dynamic neural field (DNF) model that was manipulated to replicate the behavioral performances of younger and older adults in a change detection task. Although previous work has successfully modeled children and younger adult VWM performance, this study represents the first attempt to model older adult VWM performance within the DNF architecture. In the behavioral task, older adults performed worse than

younger adults and exhibited a characteristic response bias that favored “same” over “different” responses. The DNF model was modified to capture the age group differences, with three parameter manipulations producing the best fit for the behavioral performances. The best-fitting model suggests that older adults operate through altered excitatory and inhibitory coupling and decreased inhibitory signals, resulting in wider and weaker neural signals. These results support a dedifferentiation account of brain aging, with older adults operating with wider and weaker neural signals because of decreased intracortical inhibition rather than increased stochastic neural noise. ■

## INTRODUCTION

One of the most consistent areas of cognitive decline for older adults is visual working memory (VWM), a critically important function that allows the temporary storage and retrieval of short-term visual representations. VWM is essential for keeping track of objects in a dynamic environment and detecting changes in objects when they occur. The canonical measure of VWM has been the change detection task, in which participants are briefly shown an initial stimulus display, followed by a blank screen mask, and then quickly followed by a test display that may or may not match the initial display. Participants indicate whether the test display matches (“same”) or differs (“different”) from the initial stimuli display.

Older adults have marked declines in VWM (Brockmole & Logie, 2013) and appear particularly susceptible to failures in change detection (Ko et al., 2014; Sander, Werkle-Bergner, & Lindenberger, 2011; Costello, Madden, Mitroff, & Whiting, 2010; Caird, Edwards, Creaser, & Horrey, 2005). Discerning the specific causal mechanisms for this age effect is complicated by the fact that age-related changes in VWM have been identified at multiple processing stages, including the encoding, maintenance, and recall of stimuli sets (Read, Rogers, & Wilson, 2016; Schwarzkopp, Mayr, & Jost, 2016; Ko et al., 2014; Peich, Husain, & Bays, 2013; Jost, Bryck, Vogel, & Mayr, 2011; Gazzaley et al., 2008; Fabiani, Low, Wee, Sable, & Gratton,

2006; Mitchell, Johnson, Raye, & D’Esposito, 2000; Mitchell, Johnson, Raye, Mather, & D’Esposito, 2000). The effect of aging, in other words, may not be tied to a particular processing stage but instead point to a global deterioration of the quality of VWM representations. For instance, Noack, Lövdén, and Lindenberger (2012) identified an age-related decline in representational precision in a change detection task that assessed color–location detectability. Bayesian mixed models applied to the behavioral data found an age-related increase in discriminable dispersion (i.e., reduced distinctiveness of the neural representations for visual features) at the higher set sizes (SSs). Such reductions in VWM representation quality are thought to produce a reduced signal-to-noise ratio and thereby decrease efficiency in change detection. Similarly, Pertzov, Heider, Liang, and Husain (2015) found that older adult VWM performance decreases when even only one item was assessed, indicating that their VWM representations were overall less precise, an effect exacerbated with an increased SS.

## Neural Basis of Age-related Changes to VWM

The underlying neural basis for the processing stages engaged during change detection is distributed across multiple cortical systems, including frontal, parietal, and temporal areas (see Ma, Husain, & Bays, 2014, for a review). Neural factors operative in age-related changes in VWM point to a failure to coordinate the brain regions

<sup>1</sup>University of Hartford, <sup>2</sup>University of Tennessee

responsible for efficient performance (Salthouse, 2011). Diffusion tensor imaging studies have documented age-related declines in the white matter pathways that would effectively connect the different brain regions necessary for VWM (Zahr, Rohlfing, Pfefferbaum, & Sullivan, 2009). Neural factors may also be related to changes in local regions of cortex. Aging effects have been documented on the structure of frontal cortex, which is associated with age-related working memory (WM) decline (Heinzel, Lorenz, Duong, Rapp, & Deserno, 2017; Nissim et al., 2017).

Perhaps, in response to such structural issues, older adult brains display characteristic patterns of functional overactivation. For example, Wijekumar, Magnotta, and Spencer (2017) reported increased frontal activation in an elderly group of participants relative to a group of young adults during a change detection task. Such changes in activation have been interpreted as reflecting compensatory processes associated with aging. Indeed, there is abundant evidence for compensatory recruitment in older adults particularly within the frontal cortex (Reuter-Lorenz & Cappell, 2008; Reuter-Lorenz & Lustig, 2005). Older adults have also been found to draw on both frontal areas more so than posterior regions (Davis, Dennis, Daselaar, Fleck, & Cabeza, 2008) and greater bilateral regional activity under conditions in which younger adults only require unilateral activations (Cabeza, 2002).

Mechanistically, age-related decline in VWM may reflect a decline in the specificity of neural populations coding for remembered items, resulting in broader activation for visual representations. This account is known as dedifferentiation (Park, Polk, Mikels, Taylor, & Marshuetz, 2001) and is thought to arise from one of two potential mechanisms. First, older adults may operate with a reduced signal-to-noise ratio, resulting in noisier mental representations that lack stimulus specificity (Li, Lindenberger, & Sikstrom, 2001). Evidence for an age-related increase in neural noise has been found in both animal (Schmoleky, Wang, Pu, & Leventhal, 2000) and human (Roski et al., 2014; Arena, Hutchinson, Shimozaki, & Long, 2013; Goh, 2011) models. For example, neural network modeling has found that increased noise at the synaptic level translates into less-defined mental representations (Braver & Barch, 2002; Li & Sikström, 2002; Li et al., 2001; Li, Lindenberger, & Frensch, 2000). In this case, neuronal noise would reflect the fluctuations of firing rates that have been documented under WM conditions in animal models (Shafi et al., 2007). Indeed, Welford's (1981, 1984) influential neural noise hypothesis argues that neural noise is a central influence on cognitive aging due to a variety of physiological changes that occur to the neural tissue. Second, aging is also thought to yield degeneration of the intracortical inhibition that can allow for the constrained activation patterns needed for precise representation of the stimuli features. Supporting this idea is evidence that older participants display decreased selectivity in visual processing areas and higher levels of spontaneous (non-

selective) activity (Yang et al., 2008; Schmoleky et al., 2000). Cortical overactivity in older adults, in other words, may reflect neural populations that are less inhibited (relative to younger adults) and that respond with wider (i.e., less precise) excitation patterns.

As this summary indicates, there is substantial evidence concerning the cognitive, neural, and systems level changes associated with age-related impairments of VWM. However, it is not clear how or why the neural dynamics explained above would give rise to the pattern of decline in older adult VWM abilities. Explaining what specific neurocognitive dynamics are responsible for this brain-behavior relationship requires a bridge theory that can specify how neural processes give rise to cognitive functioning. One way to explore these possibilities lies in computational modeling. Modifications to structured mathematical models can simulate age group performances in change detection, and the resulting model architecture can offer insight into how neural factors produce patterns of performance as a function of aging.

This is the theoretical justification for the current study, which will apply a dynamic neural field (DNF) model to simulate older and younger adult change detection performance to probe whether this model can provide insight to the neural processes underlying neurocognitive decline in older age. Although DNF models have been used to simulate and predict the aspects of VWM from infancy to young adulthood (Simmering & Patterson, 2012; Perone, Simmering, & Spencer, 2011; Schutte & Spencer, 2009), to date, they have never been applied to an older adult population during VWM performance.

### **Dynamic Field Theory**

The DNF model of VWM is composed of a set of neural fields that explain how items are encoded into WM, how representations are maintained in WM, and how items in WM are compared with items in the test array to generate a "same" or "different" response in change detection tasks (for a general review, see Johnson, Simmering, & Buss, 2014). The DNF model of change detection performance is composed of three interconnected DNFs whose activation unfolds in real time (see Figure 1). These fields interact through the dynamics of local excitations (i.e., neural units that are tuned to similar stimulus values excite one another) and lateral inhibition (i.e., neural units that are tuned to different stimulus values inhibit one another). These interactions give rise to "peaks" of activation that are a basic representational unit. The DNF model is implemented at the level of population dynamics and builds upon the concept of an activation field (for a review, see Trappenberg, 2010). Formulated at this level, the model simulates not only behavioral responses but also the associated hemodynamics (see Buss, Magnotta, Huppert, Schöner, & Spencer, under revision; Wijekumar, Ambrose, Spencer, & Curtu, 2017; Buss, Wifall, Hazeltine, & Spencer, 2015). In this way,

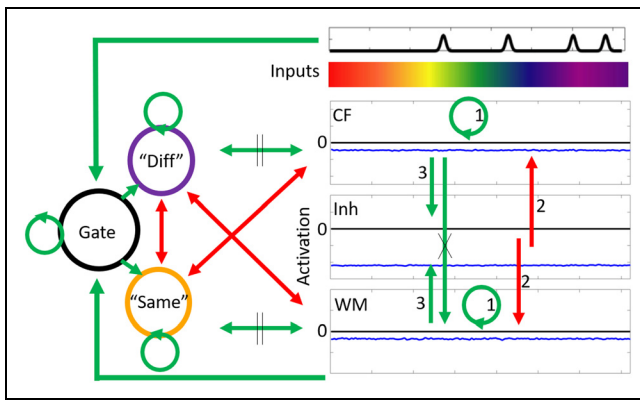


**Figure 1.** Architecture of the DNF model of change detection. Excitatory connections are marked with green arrows, whereas inhibitory connections are marked with red arrows. Parallel lines mark connections that are engaged when the gate node is activated. Crossed lines mark connections that are turned off when the gate node is activated. Numbers mark connections for reference when explaining which parameters were modified for different runs of the model.

DNF models integrate neural mechanisms, cognitive processes, and functional activation.

Figure 1 shows the architecture of the DNF model of change detection. In this figure, excitatory neural connections are marked with green arrows, whereas inhibitory neural connections are marked with red arrows. The three-layered DNF model operates as follows. First, the contrast field (CF) has local excitatory connections, meaning that neural units in this field share excitation with nearby neighbors, which are tuned to similar featural properties (see green circular arrow). Second, excitation from CF is passed to the inhibitory (Inh) and WM layers. Similar to the CF layer, the WM layer has self-excitatory connections and passes activation into the Inh layer. Third, the Inh layer passes inhibition to both the CF and WM layers. Stimuli are presented as Gaussian inputs that stimulate a subset of neural units tuned to specific feature values (see example stimuli at the top). Stimuli are given strongly into the CF layer but weakly into the WM layer. CF and Inh interact to stabilize encoding of stimuli within the CF layer. This allows CF to pass excitation into the WM layer. As representations are built within the WM layer, the Inh layer is engaged more strongly and suppresses further encoding of the items in the CF layer. Self-excitation within the WM layer interacts with lateral inhibition from the Inh layer to create self-sustaining activation that can maintain representations in the WM layer even after the stimulus has been removed. Thus, these dynamics allow for stimuli to activate neural units within the CF layer, which leads to the stable maintenance of activation within the WM layer that persists after the stimuli are removed.

The model generates “same” or “different” decisions through the activation of decision units. During the test phase of change detection, stimuli are again presented to the CF layer. If a stimulus is presented at a location that is

activated within the WM layer, then the stimulus will be strongly inhibited. However, if a stimulus is presented at a location that is not activated within the WM layer, then encoding of the stimulus will not be inhibited. To generate active decisions from the model, the “same” decision unit is coupled to the WM layer, and the “different” decision unit is coupled to the CF layer. The activation of these decision units operates in a winner-take-all fashion based on self-excitation and mutual inhibition. That is, when one unit is activated, it suppresses the activation of the other. As described below, this configuration of coupling allows the model to generate an active decision during the test phase of the change detection task.

A last component of the model is a gate node that allows the model to autonomously shift between activation modes for consolidating information into WM or comparing WM to the contents of a stimulus array to generate a decision. Specifically, a gate node receives two inputs, one in the form of a transient associated with the onset of a stimulus and another from the summed activation within the WM layer. The gate node is tuned such that it only becomes activated when there are items in WM during the transient associated with the presentation of an input. Thus, the gate node will not become activated during the memory array because WM will not yet have memory representations active. Rather, it will only become activated during the presentation of the test array once items have been consolidated into the WM layer. The gate node controls the flow of activation between the decision nodes and the CF/WM layers. When the gate node is activated, the nodes are allowed to interact with the layers, and the model generates a decision. Furthermore, the gate node prevents the updating of WM during comparison by shutting off the flow of activation from the CF layer to the WM layer.

Figure 2 demonstrates a sequence of events as the model is given a trial with four items. In Figure 2A, the inputs have been presented to the model for the encoding phase of a trial. In this panel, the model has begun to consolidate items into WM. At this time point, activation “peaks” have been built in the WM layer and the encoding of those items is being suppressed in the CF layer. Figure 2B shows the model during the test array. Two important aspects of the model’s dynamics are displayed here. First, the WM field has maintained activation associated with the items in the memory array. This is achieved through the balance of excitation and inhibition within the WM layer. Second, the CF layer is suppressed at the locations of the memory array items. This establishes a filter that will be critical for change detection during the test array. In this panel, the test array is shown for a “same” trial. All the inputs in the test array are presented at locations that are experiencing strong inhibitory suppression in CF. As a result, activation does not pierce threshold and no changes are detected. Here, the model responses “same” (see activation of decision units at the top) based on the interaction between the “same”

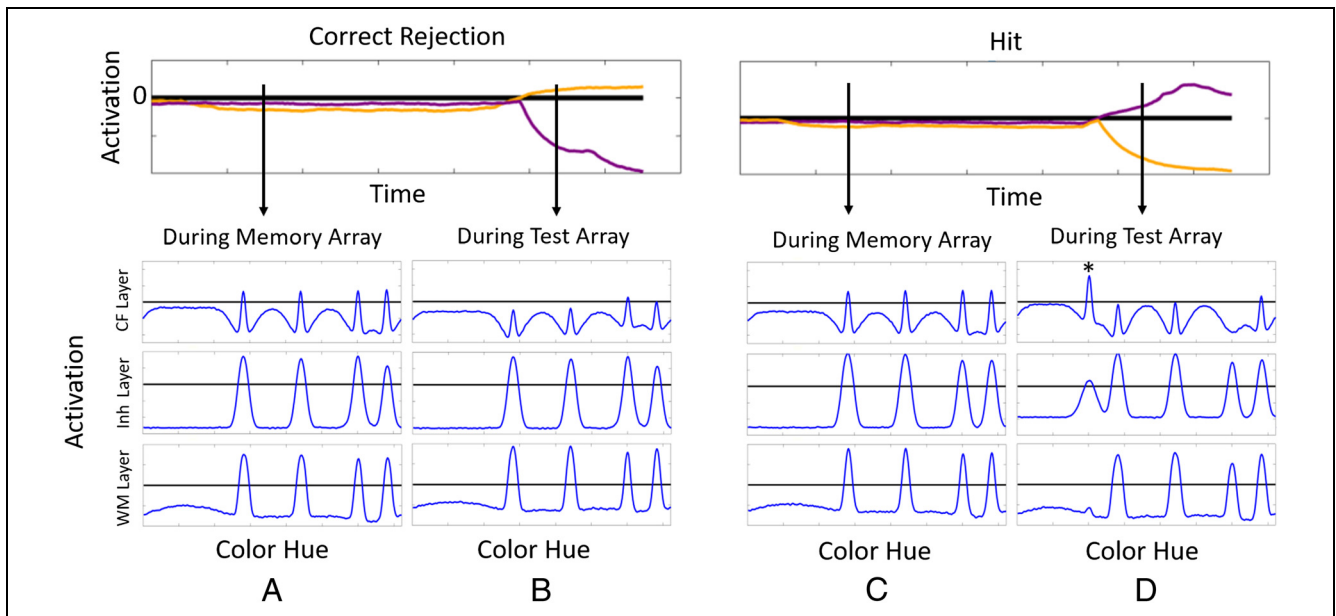


**Figure 2.** Sequence of events during correct trials in the model. The “same” decision node is plotted in orange at the top, and the “different” decision node is plotted in purple.

decision unit and the activated being received from the WM layer. In contrast, Figure 2C and D shows the model during a “different” trial. The same events unfold during the encoding phase in Figure 2C. In Figure 2D, a new item has been presented (marked with a black asterisk). This input is presented at a location that is not undergoing inhibitory suppression, and activation crosses the activation threshold, leading to a detection of a change. Here, the model responds “different” (see activation of decision units at the top).

Importantly, the model also explains sources of errors in change detection tasks. Figure 3 demonstrates the sequence of events that unfold in relation to false alarms (FAs) and miss errors. In Figure 3A, the model is again shown during the encoding phase of the trial. In Figure 3B, however, the model loses a peak during the memory delay (marked with an asterisk). During the test phase, there is no inhibitory suppression at the location of the forgotten item and the model responds “different” (see activation of decision units at the top). In contrast,

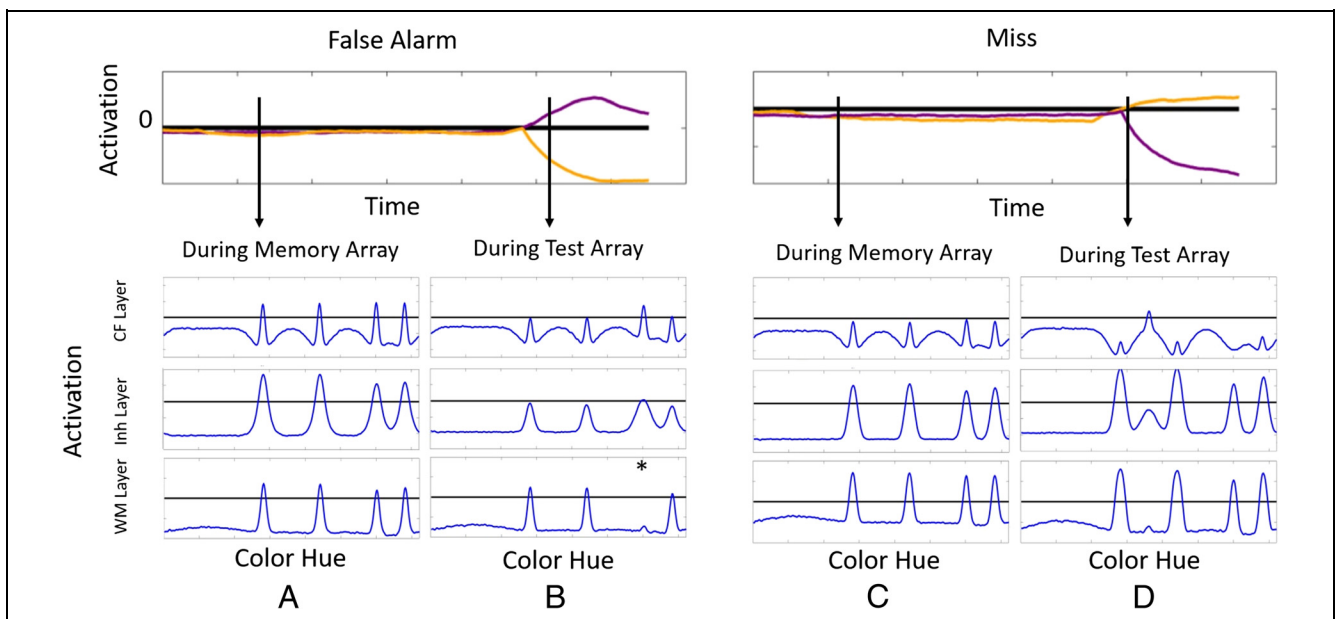


**Figure 3.** Sequence of events during incorrect trials in the model. The “same” decision node is plotted in orange at the top, and the “different” decision node is plotted in purple.

Figure 3C and D shows the model during a miss trial. Misses result from overly robust peaks of activation that lead to stronger inhibitory suppression in CF. During the test phase shown in Figure 3D, the input at a new location is partially inhibited and the model fails to generate a sufficiently strong change signal to respond “different” (see activation of decision units at the top). Thus, the DNF model explains how a common set of neural processes gives rise to both correct responses and errors. Moreover, the model also suggests that the comparison process is imperfect and errors can arise even when all items are remembered. By simulating real-time activation dynamics in a noisy, stochastic system, the model generates active decisions from trial to trial.

### Age Effects in DNF Models

The DNF model has simulated developmental improvements in change detection performance from infancy to adulthood by modifying the coupling parameters for neural interactions. Specifically, these applications have found that replicating age effects between children and younger adults requires an increase in the strength of the excitatory and inhibitory coupling between all three layers (WM, Inh, and CF). With stronger interactions, activation patterns become more stable and precise. As a result, the model maintains more peaks in WM with higher precision and becomes more sensitive to changes. These changes have reproduced developmental improvements in change detection performance and feature estimation for both color and space memory (Perone et al., 2011; Schutte & Spencer, 2009; Simmering, Schutte, & Spencer, 2008). A central question for this study is whether similar manipulations will capture the decline in older adult VWM performance.

Although older adult VWM performance has never been applied to the DNF model, a recent study by Pleger et al. (2016) applied a DNF model to simulate age-related neurocognitive decline in a perceptual discrimination task. In this task, participants experience a proprioceptive stimulus that could contain either a single point of contact or two points of contact separated by varying distances, and participants reported whether they experienced a single point or two points of contact. The result showed that the threshold of the separation needed for discriminating two points of contact increased with age, suggesting that there is an age-related decline in proprioception. To simulate this decline, Pleger et al. (2016) implemented a DNF model composed of an excitatory layer and an inhibitory layer. The excitatory layer received inputs similar to those given in the task. Either a single input was presented at a location in the field or two inputs were presented with varying separation. The model’s performance was determined by whether two peaks or a single peak was built from the inputs. To simulate differences between younger and older adults, the

synaptic tuning of the model was modified in two ways: (1) The width of self-excitation in the excitatory layer was increased (i.e., neural units shared excitation with a wider range of neighbors in the field), and (2) the width of inhibitory interactions within the excitatory layer was increased (i.e., inhibition was passed to a broader set of neurons within the excitatory field). This manipulation implemented the hypothesis that neural interactions become less precise with advanced age. With these manipulations, the model explained the quantitative details of the decline in proprioceptive discrimination in old age. Thus, in addition to explaining the complexities of performance across different trial types, DNF models have also been used to address changes in performance as a function of development and aging.

### The Current Project

The current project takes initial steps toward understanding the neural mechanisms associated with VWM decline in older age. We applied the DNF model to simulate age group differences in a behavioral VWM task to discover which manipulations to the model dynamics best explained patterns of performance differences. Below, we will first detail the behavioral change detection experiment conducted with both younger and older adults and, second, describe manipulations to a DNF model used to replicate younger and older adult human performances.

In the behavioral experiment, younger and older adults performed a 2AFC change detection task that featured simple geometrical shapes under two task conditions: an easier color task (in which shapes were held constant and color targets varied) and a more difficult shape task (in which colors were held constant and shape targets varied). Previous research has found that, in the context of change detection, color detection is easier in relation to shape detection (Wijeakumar, Magnotta, et al., 2017; Alvarez & Cavanagh, 2004) and that these two feature types are processed in differing cortical regions (Ambrose, Wijeakumar, Buss, & Spencer, 2016; Song & Jiang, 2006). These two levels of difficulty will allow us to distinguish separable neural signatures under these differing processing demands.

The DNF model is manipulated in multiple ways to achieve an optimal fit with the behavioral data. We explore several parameter manipulations of the model (including those manipulated in Pleger et al., 2016) to determine which parameter changes best explain age group differences. This project establishes the groundwork needed to explore model-based predictions in neural activation associated with VWM decline (see Buss et al., under revision; Wijeakumar, Magnotta, et al., 2017). We believe that the DNF models presented below can offer a key bridge between aging, behavioral performance, and the brain regions that underlie VWM.

## BEHAVIORAL EXPERIMENT

### Method

#### Participants

Twenty-six older adults (mean age = 70.03 years, age range = 62–86 years) and 26 younger adults (mean age = 19.88 years, age range = 18–27 years) participated in the study. Younger adults were drawn from an undergraduate student population and older adults were drawn from local newspaper ads. All research procedures were approved by the Indiana University South Bend institutional review board, and all participants provided written informed consent. Two older adults were dropped because of problems with color vision at screening, and one younger adult was dropped because of excessive errors. These dropped participants were later replaced for the 52 participant total. Testing took place in one session of approximately 1.5 hr. Participant characteristics in a range of cognitive and perceptual capacities were assessed before the change detection experiment and are presented in Table 1. All participants possessed distance visual acuity (corrected) of at least 20/40 (Bach, 1996) and at least 27 of 30 points on the Mini-Mental State Examination (MMSE; Folstein, Folstein, & McHugh, 1975).

#### Stimuli and Apparatus

Stimuli consisted of eight simple geometrical target shapes (spiral, star, triangle, I-block, circle, square, cross, and upside-down U) adapted from Simmering (2016) with eight potential RGB color values of red (255, 0, 0), yellow (255, 255, 0), green (0, 255, 0), cyan (0, 255, 255), blue (0, 0, 255), violet (238, 130, 238), white (255, 255, 255), and black (0, 0, 0). Items appeared against a gray (RGB: 150, 150, 150) background and appeared randomly around an invisible centered circular frame and against a black background. Individual items were 3.18 cm in length and appeared as  $\sim 3^\circ$  visual angle. The invisible

circular frame was designed to fit up to six items and measured 12.7 cm or  $\sim 12^\circ$  visual angle. Items were separated from one another by at least 1.27 cm or  $1.2^\circ$  visual angle, with minor spatial jitter added between them.

The experiment consisted of 240 trials, broken into a 120-trial block of the color task (in which changes were specific for color) and a 120-trial block of the shape task (in which changes were specific for shape). In the color-task-type block, all targets displayed were the spiral shape but varied based on the eight varying colors. In the shape-task-type block, all targets displayed were colored blue but varied based on the eight shape types. Across both task type blocks, different trials featured a change of only one target item from the stimuli array. Each 120-trial task block were composed of 40 trials for each SS (one, three, and five items per trial), with these 40 trials composed of 20 “same” trials (in which there were no differences between the two display screens) and 20 “different” trials (in which one item from the display was changed). For each participant and within each task type block, the SS blocks were sequentially presented from 1 to 3 to 5. The order of the task type block presentation (color/shape vs. shape/color) was counterbalanced across participants.

Participants were tested in a small quiet room designed specifically for experimental psychology research. Stimuli were presented on a Dell Optiplex 780 running Windows 7 with an Intel Core Duo CPU E8500. The monitor was a 17-in. Dell 1704FPV with a 1280  $\times$  1024 resolution. Stimuli were presented, and behavioral responses collected with E-Prime 2.0 (Psychology Software Tools, Inc.).

#### Procedure

A sample trial is illustrated in Figure 4. Participants were alerted to the upcoming trial with a centered X figure for 1000 msec, followed by a second alerting cue of a center cross hair for 1500 msec. The initial display screen then followed for 500 msec, followed by an ISI blank screen of 1200 msec. Finally, the test screen appeared in which participants responded to whether the test screen was the same or different from the initial display screen. Change trials featured changes to one item within the array at one feature dimension. Thus, in a color block, the changed target altered in color but remained constant in shape, whereas in a shape block, the changed target altered in shape but remained constant in color. Responses were made using the keyboard, with the 1-key signifying “same” and the 2-key signifying “different.” The maximum response duration was 3000 msec, and there was no feedback provided in cases of errors or no-response trials. After responding, a blank screen inter-trial interval (1000, 2500, or 3500 msec) was followed by the subsequent trial.

Participants received on-screen instructions on the task, and all participants reported verbally that they understood the instructions. The basic instructions were

**Table 1.** Participant Characteristics by Age Group for Experiment 1

	<i>M</i>		<i>SD</i>	
	<i>Younger</i>	<i>Older</i>	<i>Younger</i>	<i>Older</i>
Age (years)	19.88 <sub>a</sub>	70.08 <sub>b</sub>	2.14	7.02
Education (years)	13.12 <sub>a</sub>	15.88 <sub>b</sub>	1.31	2.29
FRACT	-0.08 <sub>a</sub>	-0.06 <sub>a</sub>	3.72	5.16
Color	13.92 <sub>a</sub>	13.40 <sub>b</sub>	0.39	0.79
MMSE	29.81 <sub>a</sub>	28.89 <sub>a</sub>	2.17	0.97

*n* = 26 per age group. FRACT = visual acuity in logMar, with 0.0 equivalent to Snellen 20/20 (Bach, 1996); Color = modified version of Dvorine color test (ref), with a maximum score of 14; MMSE = score (maximum of 30) on the MMSE (Folstein et al., 1975). Means in the same row that do not share subscripts differ by *t* test at *p* < .05.

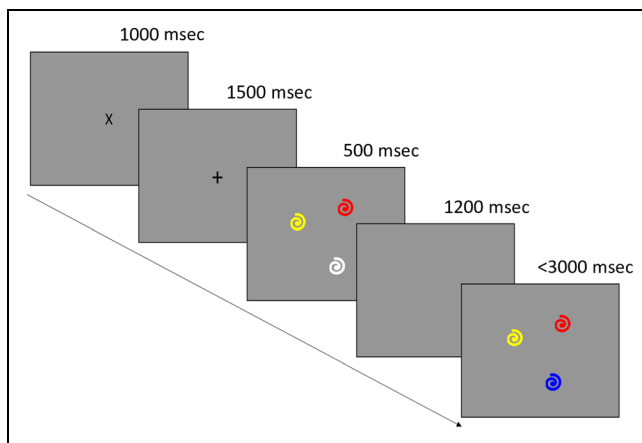


**Figure 4.** Sample of an SS3 “different” trial during a color block for the behavioral experiment.

similar across the two task type blocks, although modified for the specific target type. Participants were instructed to respond as quickly yet accurately as possible. There were no practice trials given the relative ease of the initial SS1 displays. The test took approximately 30 min to complete.

## Results

Repeated-measures ANOVA was performed on the accuracy scores with the between-participant factor of Age group (younger and older) and the within-participant factors of Difficulty (easy color task and difficult shape task), SS (one, three, and five items), and Type (“same” and “different” trial types). There was a main effect of Difficulty,  $F(1, 50) = 109.25$ , partial  $\eta^2 = .69$ ,  $p < .001$ , supporting our a priori assumption that the shape task block ( $M = 0.84$ ) would be more difficult than the color task block ( $M = 0.91$ ). Another expected main effect was SS,  $F(2, 100) = 369.53$ , partial  $\eta^2 = .88$ ,  $p < .001$ , with statistically significant differences in performance across SS1 ( $M = 0.97$ ) to SS3 ( $M = 0.90$ ) to SS5 ( $M = 0.75$ ). Difficulty and SS significantly interacted with one another,  $F(2, 100) = 51.39$ , partial  $\eta^2 = .51$ ,  $p > .001$ , with exacerbated inaccuracy by increasing SS for the shape task block relative to the color task block. There was a main effect of Type,  $F(1, 50) = 244.88$ , partial  $\eta^2 = .83$ ,  $p < .001$ , with superior performance for “same” trials ( $M = 0.95$ ) compared with “different” trials ( $M = 0.80$ ). Type and SS yielded a significant interaction,  $F(2, 100) = 186.45$ , partial  $\eta^2 = .79$ ,  $p < .001$ , with the SS effect stronger for the “different” trials (mean values: SS1 = 0.97, SS3 = 0.85, SS5 = 0.58) compared with the “same” trials (mean values: SS1 = 0.97, SS3 = 0.96, SS5 = 0.93). The difficult shape task block also yielded significantly greater errors for “different” versus “same” trials ( $M = 0.21$  greater errors) compared with the easy color task block ( $M = 0.10$  greater errors), as per a significant Difficulty  $\times$  Type interaction,  $F(1, 50) = 57.79$ , partial

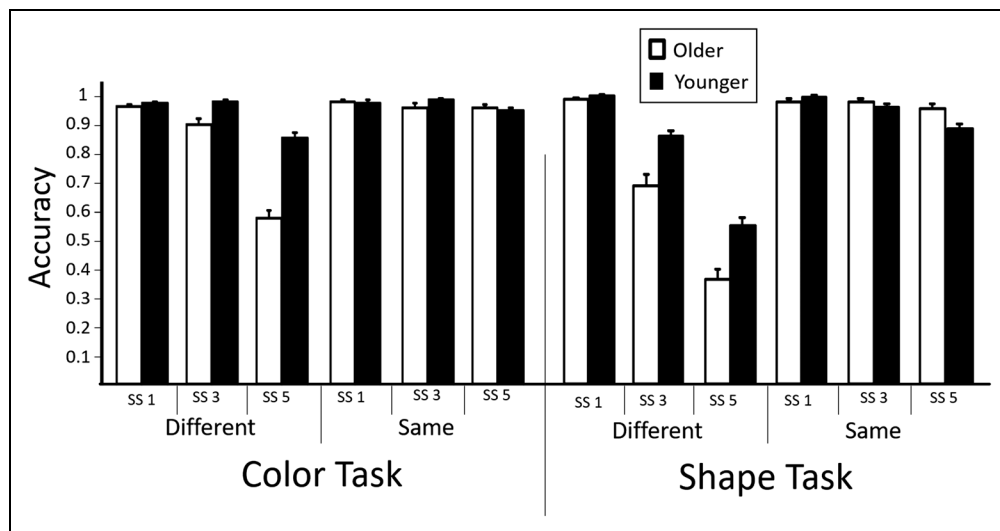
$\eta^2 = .54$ ,  $p < .001$ . The Difficulty  $\times$  SS  $\times$  Type interaction was also significant,  $F(2, 100) = 26.07$ , partial  $\eta^2 = .34$ ,  $p < .001$ , with the same–different difference increasing by SS, although more so in the difficult shape task block compared with the color task block.

The effect of Age group on accuracy yielded a number of significant effects, starting with a main effect of Age group,  $F(1, 50) = 41.61$ , partial  $\eta^2 = .45$ ,  $p < .001$ , as older adults performed worse in the task ( $M = 0.85$ ) compared with younger adults ( $M = 0.90$ ). Age group yielded multiple interactive effects. There was an Age Group  $\times$  SS interaction,  $F(2, 100) = 13.87$ , partial  $\eta^2 = .22$ ,  $p < .001$ , with the age effect exacerbated by increasing SSs. There was an Age Group  $\times$  Type interaction,  $F(1, 50) = 43.96$ , partial  $\eta^2 = .47$ ,  $p < .001$ , indicating that, whereas older adults were performing equivalently to younger adults in “same” trials ( $M_{\text{younger}} = 0.95$ ,  $M_{\text{older}} = 0.96$ ), older adults were significantly worse than younger adults under “different” trials ( $M_{\text{younger}} = 0.86$ ,  $M_{\text{older}} = 0.74$ ). There was a significant three-way interaction of Age Group  $\times$  Type  $\times$  SS,  $F(2, 100) = 25.63$ , partial  $\eta^2 = .34$ ,  $p < .001$ , indicating that age group differences in accuracy were exacerbated by increasing SS but only in the “different” trial types. This finding is illustrated in Figure 5. Thus, whereas older adults performed similarly to younger adults during same trials, during different trials, performance declined as a function of increasing VWM demands. We characterize this result as an older adult “same bias.” There was an Age Group  $\times$  SS  $\times$  Difficulty interaction,  $F(2, 100) = 5.88$ , partial  $\eta^2 = .11$ ,  $p < .01$ , indicating that the age group difference of increasing inaccuracies by SS was greater in the color task block compared with the shape task block. There were significant interactions for neither Age Group  $\times$  Difficulty nor Age Group  $\times$  Type  $\times$  Difficulty. Finally, the four-way Age Group  $\times$  Difficulty  $\times$  SS  $\times$  Type interaction was significant,  $F(2, 100) = 3.7$ , partial  $\eta^2 = .07$ ,  $p < .05$ , indicating that older adults yielded exacerbated (compared with younger adults) same–different differences by increasing SS, but more so in the difficult shape task block relative to the easier color task block.

## DNF SIMULATION

The behavioral experiment results highlight important changes in VWM performance as a function of aging. Elderly participants performed worse than younger participants as SS increased, an effect exacerbated during the different trial types and in the more challenging shape change detection task. Not only did the performance of elderly participants decline, but also their performance declined in a systematic fashion. Specifically, elderly participants exhibited a same bias in which they struggled detecting changes. In the following section, we explore different parameter manipulations to determine whether the DNF model can explain these declines in VWM performance across dimensions and age.

**Figure 5.** Mean accuracy for the behavioral experiment, broken down by SS, type, task and age group.



## Method

We initialized the model with parameters from the change detection model reported by Buss et al. (under revision). We chose to start with the model of color change detection with young adults because the DNF model has been most extensively applied to this type of data set (cf. Johnson, Spencer, Luck, & Schoner, 2009). In DNF models, the equations describing activation are nonlinear differential equations, and thus the influence of any individual parameter is dependent on all the other parameters of the model. Although it is possible that another combination of parameters could provide a reasonable starting point and an equally good fit to the young-color data set, all of the parameter adjustments we explored below did not yield a better fit to the young-color data set. Thus, we are confident that the parameters we started with are unique for the area of parameter space that we are exploring.

We initially adjusted these parameters to fit the performance of the young adults in the color change detection task (see Supplementary Information can be found at [https://abclabutk.weebly.com/uploads/6/0/4/7/60476297/jcn\\_2018.zip](https://abclabutk.weebly.com/uploads/6/0/4/7/60476297/jcn_2018.zip), for full equations and parameters). We then systematically modified the tuning of the model to test how well different mechanisms explained the pattern of responses for young adults in the more challenging shape task and older adults in both the shape and color tasks.

We then tested the role of excitatory and inhibitory interactions in the model relative to the fit to the different data sets above. Table 2 shows the 10 different models that were generated. We manipulated the shape of five interaction kernels: excitation within the model layers (marked with “1” in Figure 1), inhibition within the model layers (marked with “2” in Figure 1), excitation and inhibition (both “1” and “2”) within the model layers, to-inhibition (connections marked “3”) operative be-

tween the model layers, and noise administered both within and across model layers. These kernels are defined by two parameters corresponding to the strength and width of a Gaussian curve defining these interactions. The interaction kernels are not normalized. Both the strength and width parameters were independently manipulated for each kernel (as evident in Table 2). Note, however, that an increase in width of an interaction necessarily increased the strength at longer-range connections. For the purposes of discussing the results below, we refer to these models based on the parameters that were manipulated (e.g., the excitation width model or the to-inhibition strength model). For all the parameters that were manipulated, we modified the parameter values going both stronger and weaker in steps of 0.025 from the base parameters used to simulate the young-color data set. For example, to explore increases in a parameter value, it would be multiplied by 1.025, 1.05, and so on. To explore decreases in a parameter value, it would be multiplied by 0.975, 0.95, and so on. This allowed us to determine local maxima in the fits to the three target data sets.

Simulations were conducted in MATLAB 7.5.0 (The MathWorks, Inc.) on a PC with an Intel i7 3.5 GHz quad-core processor (the MATLAB code is available from the authors on request). For each parameter step, we conducted batches of 20 simulations (equivalent to individual participants) with 100 trials at each SS of 1, 3, and 5. Half of these trials were same trials, and half were different trials. Stimuli were given to the model to replicate the task parameters that human participants received. Stimuli consisted of Gaussian inputs centered on a set of color values. Inputs were randomly selected from an array of eight equally spaced Gaussians that had a width of 3 and an amplitude that scaled with SS (see Supplementary Information, [https://abclabutk.weebly.com/uploads/6/0/4/7/60476297/jcn\\_2018.zip](https://abclabutk.weebly.com/uploads/6/0/4/7/60476297/jcn_2018.zip)). Model dynamics were mapped to real time with 1 time step in the model equal

**Table 2.** Description of Parameters Manipulated for Each Model

<i>Model</i>	<i>Description of Manipulation</i>
Excitation width	The width of self-excitatory interactions within the CF and WM layers (connections marked “1” in Figure 1).
Excitation strength	The strength of self-excitatory interactions within the CF and WM layers (connections marked “1” in Figure 1).
Inhibition width	The width of inhibitory interactions from Inh to both CF and WM (connections marked “2” in Figure 1).
Inhibition strength	The strength of inhibitory interactions from Inh to both CF and WM (connections marked “2” in Figure 1).
Excitation and inhibition width	The width of self-excitatory interactions within the CF and WM layers (connections marked “1” in Figure 1) and the width of inhibitory interactions from Inh to both CF and WM (connections marked “2” in Figure 1).
Excitation and inhibition strength	The strength of self-excitatory interactions within the CF and WM layers (connections marked “1” in Figure 1) and the strength of inhibitory interactions from Inh to both CF and WM (connections marked “2” in Figure 1).
To-inhibition width	The width of the excitatory interactions from both CF and WM to Inh (connections marked “3” in Figure 1).
To-inhibition strength	The strength of the excitatory interactions from both CF and WM to Inh (connections marked “3” in Figure 1).
Noise width	The width of noise (stochastic fluctuations in activation) within the CF, Inh, and WM layers (not marked in Figure 1).
Noise strength	The strength of noise (stochastic fluctuations in activation) within the CF, Inh, and WM layers (not marked in Figure 1).

to 2 msec. To implement the trials, the model was given Gaussian inputs corresponding to the number of items in the memory or test array (e.g., 3 colors = 3 Gaussian inputs centered at different hue values). The experimental task featured the timing of 500 msec for the memory array, 1200 msec for the memory delay, and 1500 msec for the test phase. In the model, this translated to 250, 600, and 750 time steps, respectively. The model generated an active response on every trial determined by which decision unit became stably activated during the test array.

## Results

The model parameters were initially fit to the data from the young-color data set, based on the a priori assumption that this data set would represent superior performance. Figure 6 shows the fit of the model to the six data points in this condition. The model fit the data well with a root mean square error (RMSE) of 0.048. Thus, the model captures the pattern of responses that participants made across both same and different trials as SS increased.

To compare the fit produced by the model to the different sets of data, we computed an RMSE value for the models' fit to the test data sets. Figure 7 shows an example of how the RMSE changed as a result of the param-

eter manipulations for the excitation and inhibition width model. The RMSE was initially poor around the 0-step difference. This is expected—the parameters that fit the young-color data set fit the other data sets poorly. As these parameters were scaled, the RMSE systematically improved. This illustrates that the RMSE progressed to a local minimum, which we identified as the optimal parameter values for each data set. In the following

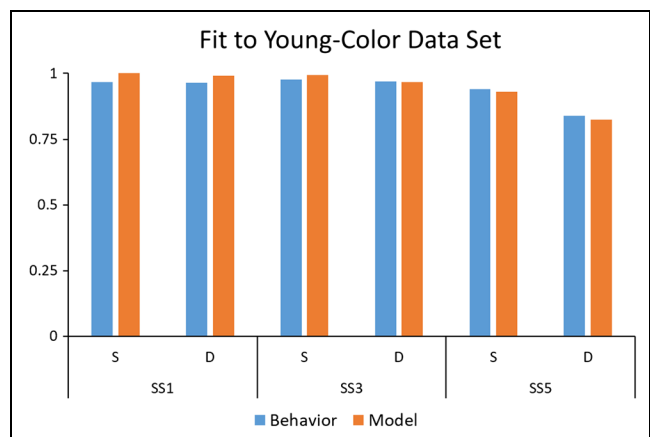
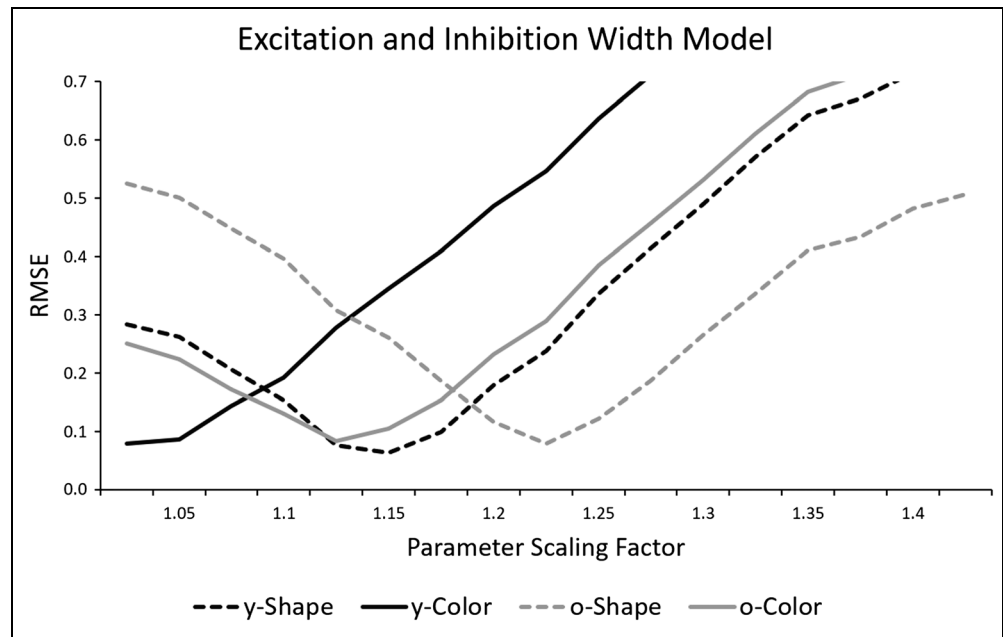


**Figure 6.** Fit of the model to the behavioral younger adult data set for the color task.

**Figure 7.** RMSEs of the models as parameters were iteratively stepped. x Axis shows the parameter scaling relative to the base parameters (1). Scaling was executed in 0.025 increments. The lowest RMSE was considered the optimum fit for the other age–task combinations. o = old; y = young.



analyses, we used the best-fitting set of parameters for each data set and each model.

Table 3 shows the best RMSE values for each data set and each model. Fits of the model to the young-shape and old-color data sets were overall very similar, ranging between 0.047 and 0.056. As can be seen in this figure, the data set that produced the highest RMSE was old-shape. The model that produced the smallest average RMSE across the three test data sets was excitation and inhibition width with a value of 0.076, followed by the inhibition width model at a value of 0.088 and the to-inhibition strength model with an RMSE of 0.100. To

statistically assess the fits of the different models, we conducted repeated-measures ANOVAs. First, we can ask whether performance across the different data sets could be explained by variation along a continuum of a specific parameter or a set of parameters. To do this, we compared the 20 runs of each model to assess their fit relative to the other model with a Model × Data Set ANOVA. We started by comparing the three best-fitting models with each other (excitation and inhibition width, inhibition width, and to-inhibition strength). In these comparisons, the fits provided by these models were not statistically different,  $F(1, 19) = 2.048, p = .138$ . However, there

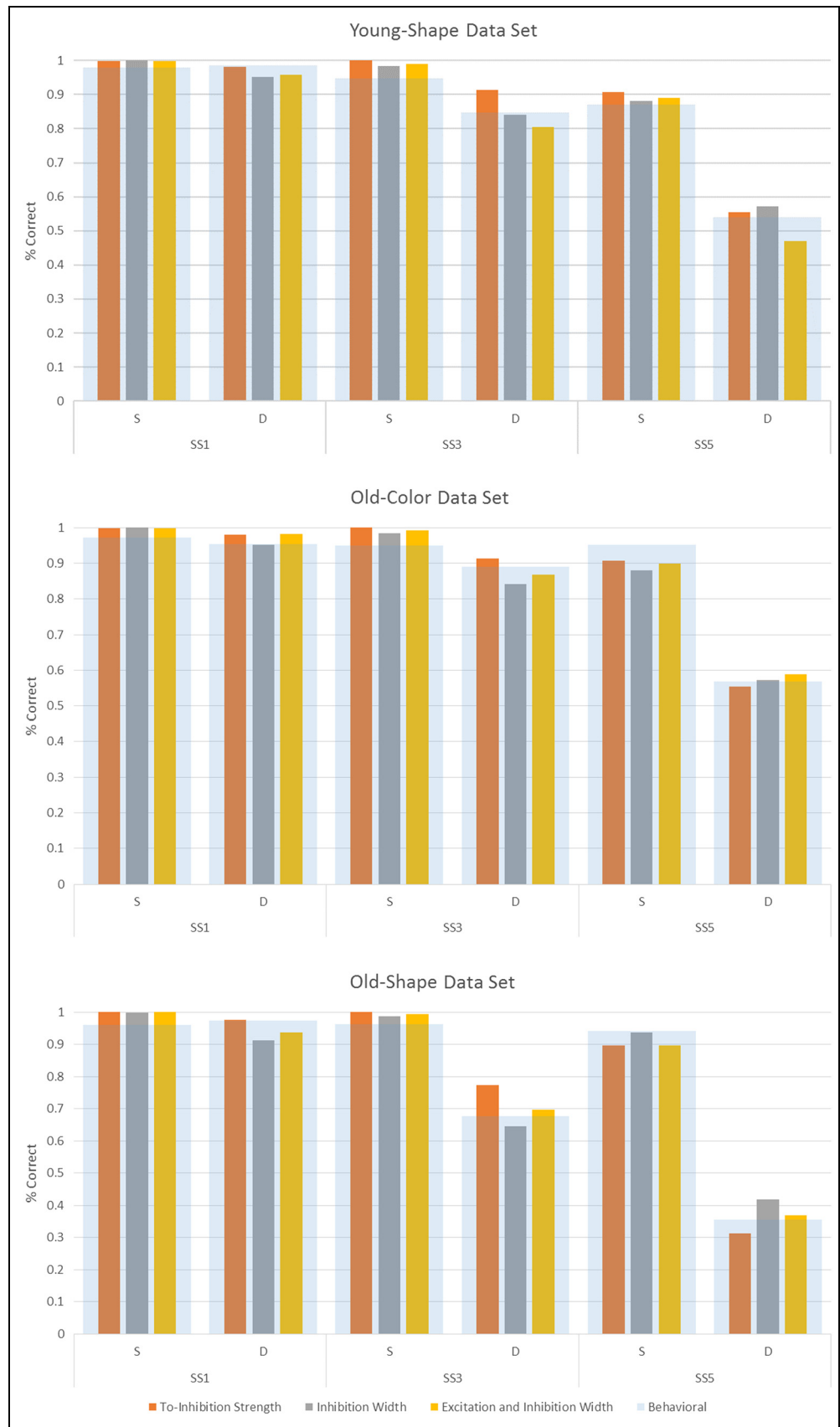
**Table 3.** Summary of the Best RMSE for Each Parameter Manipulation, With the Parameter Scaling Shown in Brackets for Each Model

Model	Young-Shape	Old-Color	Old-Shape
Excitation width	0.047 [1.150]	0.052 [1.150]	0.086 [1.250]
Excitation strength	0.050 [1.175]	0.053 [1.175]	0.091 [1.275]
Inhibition width	0.048 [1.325]	0.056 [1.300]	0.060 [1.550] <sup>a</sup>
Inhibition strength	0.061 [0.650]	0.072 [0.675]	0.144 [0.650]
Excitation and inhibition width	0.046 [1.150]	0.051 [1.125]	0.051 [1.225] <sup>b</sup>
Excitation and inhibition strength	0.057 [1.325]	0.047 [1.250]	0.072 [1.775]
To-inhibition width	0.052 [1.175]	0.056 [1.175]	0.095 [1.275]
To-inhibition strength	0.051 [0.875]	0.048 [0.900]	0.060 [0.825] <sup>b</sup>
Noise width	0.125 [1.050]	0.111 [1.050]	0.123 [1.325]
Noise strength	0.136 [1.075]	0.129 [1.050]	0.130 [1.125]

<sup>a</sup>Model that statistically outperformed the next best-fitting model.

<sup>b</sup>Models that statistically outperformed the other models for the old-shape data set ( $p < .001$ ) and were not statistically different from one another.

**Figure 8.** Pattern of accuracy from the model compared to behavioral data sets. The three best-performing models are presented here.



was a main effect of Data set,  $F(1, 19) = 15.859, p < .001$ . Follow-up analyses revealed that the old-shape data set was fit significantly more poorly than the young-shape data set,  $t(118) = 2.051, p = .001$ . No other comparisons reached significance. The poorest fitting model of this group (inhibition width model) fit the data better than the next best-fitting model (excitation width),  $F(1, 19) = 5.07, p = .030$ , supporting the cutoff we used.

Because the old-shape data set was the most challenging to fit, we performed a focused comparison on this data set. This analysis revealed that the excitation and inhibition width model had a significantly lower RMSE compared with the inhibition width model,  $t(38) = 2.421, p = .02$ , but was not significantly better than the to-inhibition strength model,  $t(38) = 1.875, p = .07$ . The fit of the to-inhibition strength model to the old-shape data set was not better than that of the inhibition width model,  $t(38) = 0.393, p = .70$ . The inhibition width model fit better than the next best-fitting model, which was the excitation and inhibition strength model,  $t(38) = 3.593, p < .01$ . Figure 8 shows the details of the models' performance across the different trial types for each data set. As can be seen, these models fit the pattern of accuracy on specific trial types well.

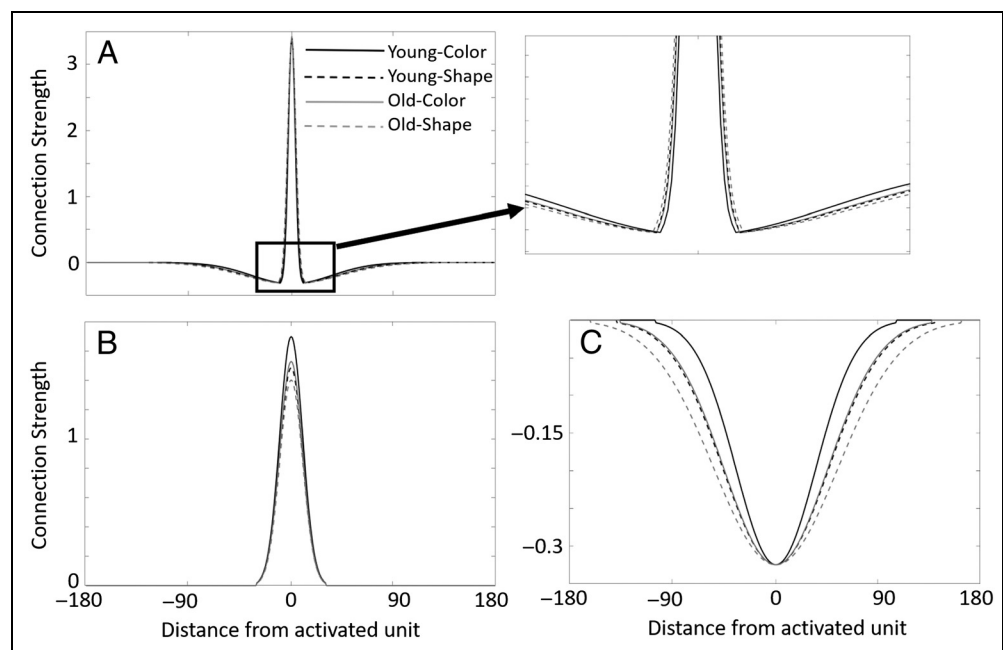
Figure 9 plots the interaction kernels used to define the shape of the neural interactions for the models that best fit the four data sets (i.e., younger color and shape, and older color and shape). In Figure 9A, the interaction kernels for the excitatory and inhibitory interactions are plotted for the excitation and inhibition width model. This illustrates the profile of local excitation and lateral inhibition interactions within the WM and CF layers. To explain changes in performance as a function of dimension and age, the interaction kernel increased in width

relative to the model that fits the young-color data set. In Figure 9B, the interaction kernels are plotted for the to-inhibition strength model. This illustrates the shape of excitatory neural interactions from the WM and CF layers into the Inh layer. To explain changes in performance as a function of dimension and age, the interaction kernel became weaker relative to the model that fits the young-color data set. Finally, Figure 9C plots the interaction kernel that was modified for the inhibition width model. This illustrates the profile of inhibitory interactions from the Inh layer to the CF and WM layers. To explain changes in performance as a function of dimension and age, the interaction kernel became wider relative to the model that fits the young-color data set.

To explore the relative contribution of these different parameters of the model, we combined the inhibition width model parameters that best explained performance in the young-shape data set and the to-inhibition strength model parameters that best explained performance in the old-color data sets to determine whether these factors could be combined to explain performance on the old-shape data set. The motivation for this comparison is to explore whether different factors could explain differences between dimensions and differences between ages. Comparison of this hybrid model against the excitation and inhibition width model relative to the old-shape data set is plotted in Figure 10. There were no significant differences in model fits between these models for this data set,  $t(19) = 0.473, p = .642$ .

Next, we explored the properties of the model associated with errors and correct responding at the highest SS (SS5), which had the most number of incorrect trials. The top row of Figure 11 plots the number of peaks within the WM layer at the end of the delay phase immediately

**Figure 9.** Visualization of interaction kernels for the three best-performing models. (A) Excitation and inhibition width with zoom-in on kernel on the right. (B) To-inhibition strength. (C) Inhibition width.



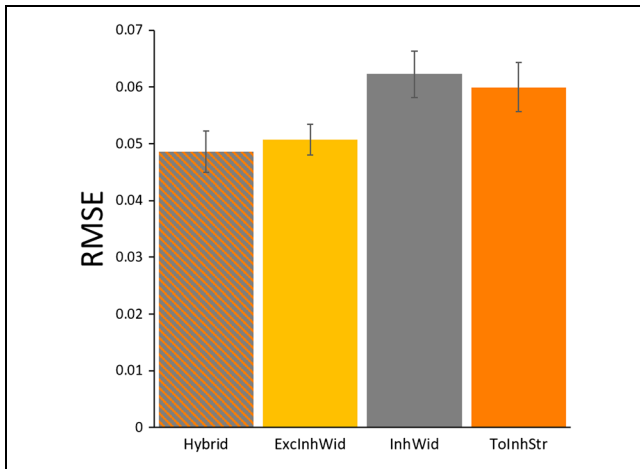


**Figure 10.** RMSE for the model fits to the old-shape data set. The three best-fitting models and a hybrid model are presented. The hybrid model combined the parameters from the inhibition width model that best fit the young-shape data set and the parameters from the to-inhibition strength model that best fit the old-color data set.

before presentation of the test array. Data are plotted for correct rejections (correct same trials), hits (correct change trials), FAs (incorrect same trials), and misses (incorrect different trials) for each data set and each model. As can be seen, the excitation and inhibition width model

and the inhibition width model had fewer peaks for shape relative to color trials and fewer peaks from old models compared with young models. However, the to-inhibition strength model produced a full set of five peaks nearly every trial for all three test data sets. In addition, the models tended to have fewer peaks on FA trials compared with other trial types. The bottom row in Figure 11 illustrates the average number of neural units participating in each peak at this same point in time of the simulation immediately before the presentation of the test array. We observed an increase in the number of activated units for the shape relative to the color simulations and for the old relative to the young simulations for the excitation and inhibition width model and the to-inhibition strength model. However, we observed a decrease in the number of units activated for all test data sets relative to the young-color data set for the inhibition width model.

These results point to three possibilities. It could be that performance across difficulty and age is explained along a continuum of parameters for the models explored here. Alternatively, the effect of dimension and age might be explained by distinct mechanistic changes to the inhibitory system: The effect of dimension was best explained by increases in the width of inhibition, and the effect of age was best explained by decreased strength of input into the inhibitory system. In this case,

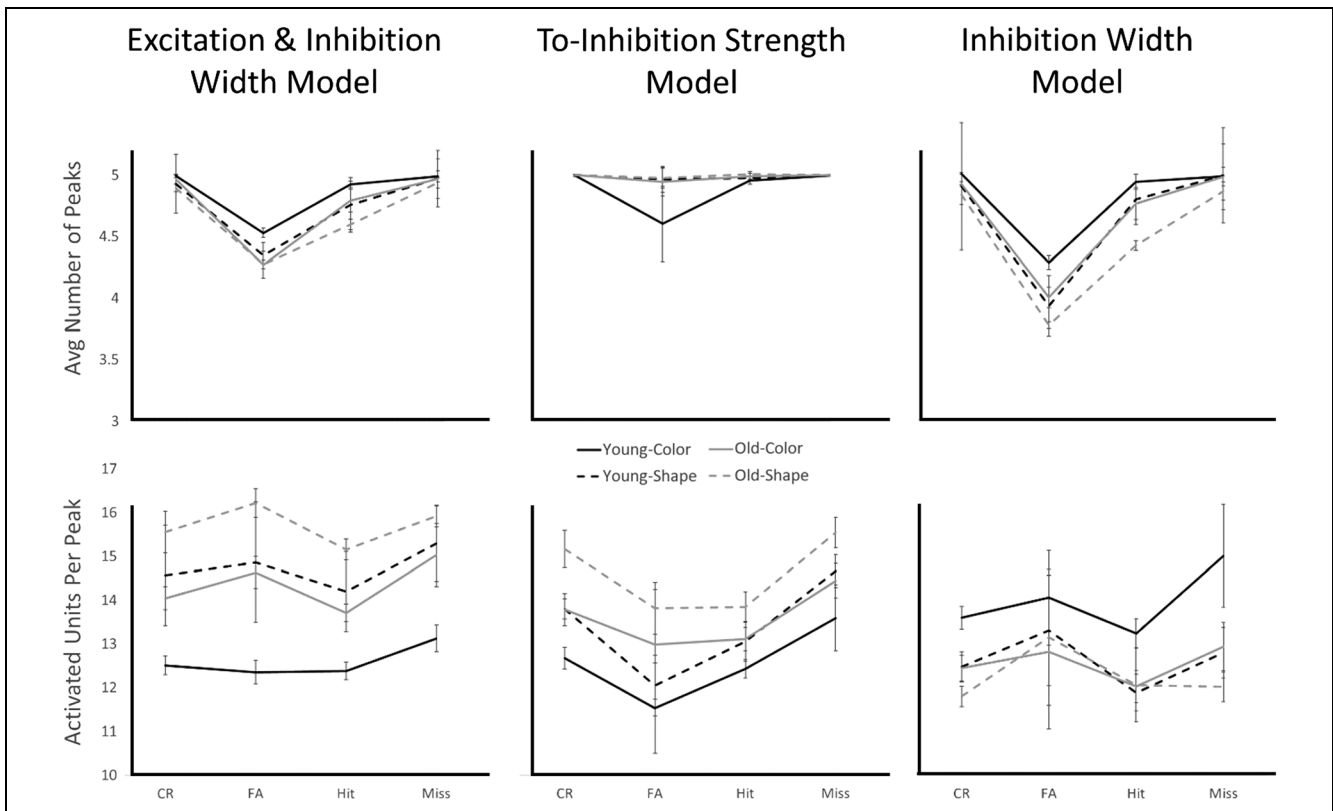


**Figure 11.** Number of peaks for each trial type (top) and number of activated units per peak (bottom) for models that best fit the young-color (solid black), young-shape (dashed black), old-color (solid gray), and old-shape (dashed gray). CR = correct rejection trials; FA = false alarm trials; Avg = average.

performance in the old-shape data set would reflect the combination of these two factors. Indeed, when these factors were combined, the model explained the behavioral data in the old-shape data set as well as the excitation and inhibition width model. Thus, model fits to these behavioral data cannot differentiate between the explanation offered by the excitation and inhibition width or to-inhibition strength models or a combination of to-inhibition strength and inhibition width manipulations. Future work can further examine age-related effects to determine if these models can be differentiated relative to their fit to behavioral data in other VWM tasks or hemodynamic data collected during VWM tasks. We further address this in the Discussion section below.

## Discussion

VWM is of critical importance to cognitive function, and its decline in older adults offers a window into age-related neural degeneration. In our VWM task, the elderly group of participants performed worse than the young adult group, with a characteristic same bias that was especially evident at higher SSs. Although both age groups responded more accurately to the same trials compared with the different trials, older adults displayed exacerbated performance decline under the “different” conditions, especially with increasing VWM (SS) loads. Furthermore, although both age groups performed worse under “different” conditions with the shape task relative to the color task, older adult decline was exacerbated under the shape task with increasing VWM demands. These results suggest that the age effect and difficulty effect may fall along a continuum. That is, declines in performance as a function of dimension and declines in performance as a function of age may arise from the same mechanism. Alternatively, it may be that distinct mechanisms mediate differences based on difficulty of the dimension and age. This is suggested by the improved fit to the old-shape behavioral data when combining the to-inhibition strength parameters that fit the old-color behavioral data (i.e., an aging effect) with the inhibition width parameters that fit the young-shape behavioral data (i.e., a dimension effect).

Our modeling results demonstrated how both of these possibilities provide viable explanations of age-related decline in VWM performance. The excitation and inhibition width model (wider excitatory and inhibitory interactions) explained the pattern of performance across dimensions and age equally well as the inhibition strength model (weaker excitatory input into the inhibitory field). Combining these models for the old-shape data set yielded an equally good fit as the other two models. Despite this relative ambiguity regarding which mechanism or mechanisms best explain performance across dimensions and age, an important contribution of the simulations presented here is to provide con-

straints on the types of mechanisms that can give rise to degenerations in performance across these factors. That is, three mechanisms provided superior fits to the performance of older adults in the shape change detection condition relative to the 10 mechanisms that were explored.

Importantly, the simulations that yielded the best fits to the data sets are consistent with various observations of the neural dynamics associated with cognitive decline. For example, older adults have well-documented declines in inhibitory control (McDowd, 1997). Our results suggest that this would be a natural consequence of the to-inhibition model, which has weaker engagement of the inhibitory field. Moreover, functional overactivation is common in older adults, particularly in frontal recruitment and bilateral activation patterns, when performing in challenging cognitive conditions (Davis et al., 2008; Cabeza, 2002). Such results are thought to arise from dedifferentiation of neural connectivity (Goh, 2011; Park et al., 2001). Dedifferentiation is generally thought to result from deterioration of the functional response, with one major neurophysiological explanation being the impairment of white matter connections allowing efficient cross-regional communication. Our results offer an important bridge between these brain and behavioral results. First, the mechanisms implemented to explain performance implemented deteriorated connectivity between neural populations, which could arise from such impairments in white matter connections. Second, a natural consequence of the excitation and inhibition width model would be the recruitment of more cortical resources with aging. Relatedly, the to-inhibition model reduced the recruitment of inhibitory signals in the models. As a consequence of this manipulation, excitation will tend to be stronger and more diffuse. In this regard, our modeling results are consistent with the dedifferentiation account of aging given the broader or weaker connectivity implemented between neural populations.

Our model results also argue against a currently dominant theoretical perspective on the decline in cognitive processes as a function of aging, which suggests that an increase in neural noise is a primary mechanism of cognitive decline (Welford, 1984). The model that directly manipulated the properties of noise in the model did not yield systematic changes in the quality of the model's fit to the behavioral data. It is possible, though, that the models that were able to explain the behavioral data could yield representations that are less precise and less consistent over time. For example, the inhibition and excitation width model made neural interactions wider, which means that more neurons would become engaged for a given representation. In this case, “noise” pertains to the neural response width, rather than stochastic noise pervading the model. On the basis of our results, an age-related increase in neural noise would reflect disrupted connectivity between model layers (and, by

extension, between cortical regions) necessary for efficient performance. By our account, neural noise is a secondary expression of alterations to the excitation and inhibition width changes in the older model that resulted in broader neural interactions. This means that specific colors and shapes are encoded more diffusely and require greater population activation to achieve the coded representation.

Our results are less specific with regard to compensatory models of cognitive aging (such as HAROLD and PASA), although this reflects the limitations of the change detection task. Compensatory explanations typically refer to increased top-down attention needed to offset age-related declines in sensory processing. Our change detection task design offered minimal top-down control, given that the participants had no knowledge of the targets beyond the prechange and postchange comparison. Therefore, although our results are strongly supportive of neural accounts such as dedifferentiation, they are neutral on the question of age-related compensatory mechanisms.

The current study is limited in the degree to which we can specify cortical mechanisms at work in the age effect of VWM, for our data types are behavioral and computational, rather than neurophysiological. Nevertheless, our results speak indirectly to support investigations in the neurophysiological causes of age effects. Our modeling results found an age-related decrease in inhibitory signals, similar to Schmolesky et al. (2000) who found that the reduced stimulus selectivity in aged rhesus monkeys was due to deterioration of intracortical inhibition. They hypothesized that this increased excitability in the older monkeys was due to reductions in the neurotransmitter GABA, although other researchers have targeted the dopamine system operative within frontal cortical regions. Optimal WM performance has been linked to the inhibitory D1 receptors in the pFC (cf. Durstewitz, Seamans, & Sejnowski, 2000; Muller, von Cramon, & Pollmann, 1998; Seamans, Floresco, & Phillips, 1998), and reductions in dopamine levels in older adults have been linked with a decrease in cognitive processes including WM (for a review, cf. Backman, Nyberg, Lindenberger, Li, & Farde, 2006). Although speculative, our work is largely consistent with the possibility that the age effect in VWM is due to deteriorating inhibitory signals operative within frontal regions.

However, this project is only a first step in understanding how the dynamic connectivity between neural layers can account for the age-related decline in VWM. One aspect of performance that has been explored with young adults is the influence of metric similarity of items in WM. This work has demonstrated that change detection is enhanced when memory items are close together in feature space compared with when they are far apart (Johnson et al., 2009). Furthermore, items that are close together in feature space tend to repel one another when probed with a color estimation procedure such that color estima-

tion responses are biased away from the metrically similar item (Johnson, Ambrose, van Lamsweerde, Dineva, & Spencer, submitted). Johnson et al. (submitted) demonstrated that the neural interactions implemented by the DNF model of VWM replicated this pattern of color estimation data. Thus, future work can probe differences in color estimation between young and old adults. Results from a study such as this can provide further tests of the mechanisms proposed here to explain differences between age and feature dimensions in VWM.

Previous work suggests that the DNF model can serve as an essential bridge between behavioral and functional neural data. The equivocal results regarding the fit of the model to the behavioral data point to the importance of model-based fMRI studies. For instance, we could extend the simulation results here to generate hemodynamic responses from the different models that fit the behavioral data with superior RMSEs. Using an established method of simulating hemodynamic responses from the literature on the neurophysiological basis of the hemodynamic response (Deco, Rolls, & Horwitz, 2004; Logothetis, Pauls, Augath, Trinath, & Oeltermann, 2001), Buss et al. (under revision) applied the DNF model to explain both young adults' performance in a change detection task and their associated neural measures obtained from fMRI. In this project, the model was used not only to simulate patterns of behavioral responses from young adults but also to predict patterns of hemodynamic responses. These analyses revealed that the pattern of hemodynamic activation generated by different components of the model predicted patterns of activation across distinct neural networks previously implicated in VWM.

Future work can use this model-based approach in conjunction with fMRI to further constrain the models explored here and better understand the functional significance of changes in cortical activation. That is, we can explore the cognitively functional aspects of shifts in neural activation using the model to bridge between behavioral and neural data. First, we could identify regions that show changes in activation between young and old adults across stimulus dimensions. Second, we can determine which model (i.e., neural mechanism) best predicts these patterns of activation across age and stimulus type. Third, we can then explore which model components show correspondence with regions in which activation shifts as a function of aging. For example, if these regions show correspondence with the WM layer, this may suggest that shifts in activation result from sustained maintenance processes. However, if these regions show correspondence with the CF layer, this may suggest that these regions are compensating during the comparison process. Finally, these regions may show correspondence with the decision units in the model, which may implicate these regions in the decision-making process and the allocation of attention to memory and comparison processes. Future work applying a model-based approach to fMRI with aging populations will be required to address these issues.

To conclude, the results presented here point toward a limited subset of neural mechanisms that can plausibly explain VWM decline across stimulus difficulty and aging factors. The model results suggest that age-related declines arise not from circumscribed effects to specific stages of processing or cognitive components but instead from degradation to the dynamic neural processes that give rise to representations in VWM and the decision-making process that compares the contents of VWM to stimuli in the environment. Future work with this modeling framework will focus on neural dynamics across stimulus difficulty and aging to examine whether the model can shed light on the pattern of activation across these factors.

Reprint requests should be sent to Matthew C. Costello, Department of Psychology, University of Hartford, 200 Bloomfield Avenue, West Hartford, CT 06117, or via e-mail: mcostello@hartford.edu.

## REFERENCES

- Alvarez, G. A., & Cavanagh, P. (2004). The capacity of visual short-term memory is set both by visual information load and by number of objects. *Psychological Science, 15*, 106–111.
- Ambrose, J. P., Wijekumar, S., Buss, A. T., & Spencer, J. P. (2016). Feature-based change detection reveals inconsistent individual differences in visual working memory capacity. *Frontiers in Systems Neuroscience, 10*, 1–10.
- Arena, A., Hutchinson, C. V., Shimozaki, S. S., & Long, M. D. (2013). Visual discrimination in noise: Behavioural correlates of age-related cortical decline. *Behavioural Brain Research, 243*, 102–108.
- Bach, M. (1996). The Freiburg Visual Acuity Test—Automatic measurement of visual acuity. *Optometry and Vision Science, 73*, 49–53.
- Backman, L., Nyberg, L., Lindenberger, U., Li, S.-C., & Farde, L. (2006). The correlative triad among aging, dopamine, and cognition: Current status and future prospects. *Neuroscience & Biobehavioral Reviews, 20*, 791–807.
- Braver, T. S., & Barch, D. M. (2002). A theory of cognitive control, aging cognition, and neuromodulation. *Neuroscience & Biobehavioral Reviews, 26*, 809–817.
- Brockmole, J. R., & Logie, R. H. (2013). Age-related change in visual working memory: A study of 55,753 participants aged 8–75. *Frontiers in Psychology, 4*, 12.
- Buss, A. T., Magnotta, V., Huppert, T. J., Schöner, G., & Spencer, J. P. (under revision). How do neural processes give rise to cognition? Simultaneously predicting brain and behavior with a dynamic neural of visual working memory.
- Buss, A. T., Wifall, T., Hazeltine, E., & Spencer, J. P. (2015). Integrating the behavioral and neural dynamics of response selection in a dual-task paradigm: A dynamic neural field model of Dux et al. (2009). *Journal of Cognitive Neuroscience, 26*, 334–351.
- Cabeza, R. (2002). Hemispheric asymmetry reduction in older adults: The HAROLD model. *Psychology and Aging, 17*, 85–100.
- Caird, J. K., Edwards, C. J., Creaser, J. I., & Horrey, W. J. (2005). Older driver failures of attention at intersections: Using change blindness methods to assess turn decision accuracy. *Human Factors, 47*, 235–249.
- Costello, M. C., Madden, D. J., Mitroff, S. R., & Whiting, W. L. (2010). Age-related decline of visual processing components in change detection. *Psychology and Aging, 25*, 356–368.
- Davis, S. W., Dennis, N. A., Daselaar, S. M., Fleck, M. S., & Cabeza, R. (2008). Que pasa? The posterior–anterior shift in aging. *Cerebral Cortex, 18*, 1201–1209.
- Deco, G., Rolls, E. T., & Horwitz, B. (2004). “What” and “where” in visual working memory: A computational neurodynamical perspective for integrating fMRI and single-neuron data. *Journal of Cognitive Neuroscience, 16*, 683–701.
- Durstewitz, D., Seamans, J. K., & Sejnowski, T. J. (2000). Neurocomputational models of working memory. *Nature Neuroscience, 3*, 1184–1191.
- Fabiani, M., Low, K. A., Wee, E., Sable, J. J., & Gratton, G. (2006). Reduced suppression or labile memory? Mechanisms of inefficient filtering of irrelevant information in older adults. *Journal of Cognitive Neuroscience, 184*, 637–650.
- Folstein, M. F., Folstein, S. E., & McHugh, P. R. (1975). “Minimal state”: A practical method for grading the cognitive state of patients for the clinician. *Journal of Psychiatric Research, 12*, 189–198.
- Gazzaley, A., Clapp, W., Kelly, J., McEvoy, K., Knight, R. T., & D’Esposito, M. (2008). Age-related top–down suppression deficit in the early stages of cortical visual memory processing. *Proceedings of the National Academy of Sciences, U.S.A., 105*, 13122–13126.
- Goh, J. O. S. (2011). Functional dedifferentiation and altered connectivity in older adults: Neural accounts of cognitive aging. *Aging and Disease, 2*, 30–48.
- Heinzel, S., Lorenz, R. C., Duong, Q. L., Rapp, M. A., & Deserno, L. (2017). Prefrontal–parietal effective connectivity during working memory in older adults. *Neurobiology of Aging, 57*, 18–27.
- Johnson, J. S., Ambrose, J. P., van Lamsweerde, A. E., Dineva, E., & Spencer, J. P. (submitted). Neural interactions in working memory cause variable precision and similarity-based feature repulsion.
- Johnson, J. S., Simmering, V. R., & Buss, A. T. (2014). Beyond slots and resources: Grounding cognitive concepts in neural dynamics. *Attention, Perception, & Psychophysics, 76*, 1630–1654.
- Johnson, J. S., Spencer, J. P., Luck, S. J., & Schoner, G. A. (2009). Dynamic neural field model of visual working memory and change detection. *Psychological Science, 20*, 568–577.
- Jost, K., Bryck, R. L., Vogel, E. K., & Mayr, U. (2011). Are old adults just like low working memory young adults? Filtering efficiency and age differences in visual working memory. *Cerebral Cortex, 21*, 1147–1154.
- Ko, P. C., Duda, B., Hussey, E., Mason, E., Molitor, R. J., Woodman, G. F., et al. (2014). Understanding age-related reductions in visual working memory capacity: Examining the stages of change detection. *Attention, Perception, & Psychophysics, 76*, 2015–2030.
- Li, S. C., Lindenberger, U., & Frensch, P. A. (2000). Unifying cognitive aging: From neuromodulation to representation to cognition. *Neurocomputing, 32*, 879–890.
- Li, S. C., Lindenberger, U., & Sikstrom, S. (2001). Aging cognition: From neuromodulation to representation. *Trends in Cognitive Science, 5*, 479–486.
- Li, S. C., & Sikström, S. (2002). Integrative neurocomputational perspectives on cognitive aging, neuromodulation, and representation. *Neuroscience & Biobehavioral Reviews, 26*, 795–808.
- Logothetis, N. K., Pauls, J., Augath, M., Trinath, T., & Oeltermann, A. (2001). Neurophysiological investigation of the basis of the fMRI signal. *Nature, 412*, 150–157.
- Ma, W. J., Husain, M., & Bays, P. M. (2014). Changing concepts of working memory. *Nature Neuroscience, 17*, 347–356.
- McDowd, J. M. (1997). Inhibition in attention and aging. *Journals of Gerontology, Series B, Psychological Sciences and Social Sciences, 52*, 265–273.

- Mitchell, K. J., Johnson, M. K., Raye, C. L., & D'Esposito, M. (2000). fMRI evidence of age-related hippocampal dysfunction in feature binding in working memory. *Cognitive Brain Research*, *10*, 197–206.
- Mitchell, K. J., Johnson, M. K., Raye, C. L., Mather, M., & D'Esposito, M. (2000). Aging and reflective processes of working memory: Binding and test load deficits. *Psychology and Aging*, *15*, 527–541.
- Muller, U., von Cramon, D. Y., & Pollmann, S. (1998). D1- versus D2-receptor modulation of visuospatial working memory in humans. *Journal of Neuroscience*, *18*, 2720–2728.
- Nissim, N. R., O'Shea, A. M., Bryant, V., Porges, E. C., Cohen, R., & Woods, A. J. (2017). Frontal structural neural correlates of working memory performance in older adults. *Frontiers in Aging Neuroscience*, *8*, 1–9.
- Noack, H., Lövdén, M., & Lindenberger, U. (2012). Normal aging increases discriminial dispersion in visuospatial short-term memory. *Psychology and Aging*, *27*, 627–637.
- Park, D. C., Polk, T. A., Mikels, J. A., Taylor, S. F., & Marshuetz, C. (2001). Cerebral aging: Integration of brain and behavioral models of cognitive function. *Dialogues in Clinical Neuroscience*, *3*, 151–165.
- Peich, M.-C., Husain, M., & Bays, P. M. (2013). Age-related decline of precision and binding in visual working memory. *Psychology and Aging*, *28*, 729–743.
- Perone, S., Simmering, V. R., & Spencer, J. P. (2011). Stronger neural dynamics capture changes in infants' visual working memory capacity over development. *Developmental Science*, *14*, 1379–1392.
- Pertsov, Y., Heider, M., Liang, Y., & Husain, M. (2015). Effects of healthy aging on precision and binding of object location in visual short term memory. *Psychology and Aging*, *30*, 26–35.
- Pleger, B., Wilimzig, C., Nicolas, V., Kalisch, T., Ragert, P., Tegenthoff, M., et al. (2016). A complimentary role of intracortical inhibition in age-related tactile degradation and its remodelling in humans. *Scientific Reports*, *6*, 1–15.
- Read, C. A., Rogers, J. M., & Wilson, P. H. (2016). Working memory binding of visual object features in older adults. *Neuropsychology, Development, and Cognition, Series B: Aging, Neuropsychology, and Cognition*, *23*, 263–281.
- Reuter-Lorenz, P. A., & Cappell, K. A. (2008). Neurocognitive aging and the compensation hypothesis. *Current Directions in Psychological Science*, *17*, 177–182.
- Reuter-Lorenz, P. A., & Lustig, C. (2005). Brain aging: Reorganizing discoveries about the aging mind. *Current Opinion in Neurobiology*, *15*, 245–251.
- Roski, C., Caspers, S., Lux, S., Hoffstaedter, F., Bergs, R., Amunts, K., et al. (2014). Activation shift in elderly subjects across functional systems: An fMRI study. *Brain Structure & Function*, *219*, 707–718.
- Salthouse, T. A. (2011). Neuroanatomical substrates of age-related decline. *Psychological Bulletin*, *137*, 753–784.
- Sander, M. C., Werkle-Bergner, M., & Lindenberger, U. (2011). Binding and strategic selection in working memory: A lifespan dissociation. *Psychology and Aging*, *26*, 612–624.
- Schmolecky, M. T., Wang, Y., Pu, M., & Leventhal, A. G. (2000). Degradation of stimulus selectivity of visual cortical cells in senescent rhesus monkeys. *Nature Neuroscience*, *3*, 384–390.
- Schutte, A. R., & Spencer, J. P. (2009). Tests of the dynamic field theory and the spatial precision hypothesis: Capturing a qualitative developmental transition in spatial working memory. *Journal of Experimental Psychology: Human Perception and Performance*, *35*, 1698–1725.
- Schwarzkoopp, T., Mayr, U., & Jost, K. (2016). Early selection versus late correction: Age-related differences in controlling working memory contents. *Psychology and Aging*, *31*, 430–441.
- Seamans, J. K., Floresco, S. B., & Phillips, A. G. (1998). D1 receptor modulation of hippocampal–prefrontal cortical circuits integrating spatial memory with executive functions in the rat. *Journal of Neuroscience*, *18*, 1613–1621.
- Shafi, M., Zhou, Y., Quintana, J., Chow, C., Fuster, J., & Bodner, M. (2007). Variability in neuronal activity in primate cortex during working memory tasks. *Neuroscience*, *146*, 1082–1108.
- Simmering, V. R. (2016). Working memory capacity in context: Modeling dynamic processes of behavior, memory and development. *Monographs of the Society for Research in Child Development*, *81*, 7–24.
- Simmering, V. R., & Patterson, R. (2012). Models provide specificity: Testing a proposed mechanism of visual working memory capacity development. *Cognitive Development*, *27*, 419–439.
- Simmering, V. R., Schutte, A. R., & Spencer, J. P. (2008). Generalizing the dynamic field theory of spatial cognition across real and developmental time scales. *Brain Research*, *1202*, 68–86.
- Song, J. H., & Jiang, Y. (2006). Visual working memory for simple and complex features: An fMRI study. *Neuroimage*, *30*, 963–972.
- Trappenberg, T. P. (2010). *Fundamentals of computational neuroscience* (2nd ed). Oxford: Oxford University Press.
- Welford, A. T. (1981). Signal, noise, performance, and age. *Human Factors*, *23*, 97–109.
- Welford, A. T. (1984). Between bodily changes and performance: Some possible reasons for slowing with age. *Experimental Aging Research*, *10*, 73–88.
- Wijeakumar, S., Ambrose, J. P., Spencer, J. P., & Curtu, R. (2017). Model-based functional neuroimaging using dynamic neural fields: An integrative cognitive neuroscience approach. *Journal of Mathematical Psychology*, *76*, 212–235.
- Wijeakumar, S., Magnotta, V. A., & Spencer, J. P. (2017). Modulating perceptual complexity and load reveals degradation of the visual working memory network in ageing. *Neuroimage*, *157*, 464–475.
- Yang, Y., Liang, Z., Li, G., Wang, Y., Zhou, Y., & Leventhal, A. G. (2008). Aging affects contrast response functions and adaptation of middle temporal visual area neurons in rhesus monkeys. *Neuroscience*, *156*, 748–757.
- Zahr, N. M., Rohlfing, T., Pfefferbaum, A., & Sullivan, E. V. (2009). Problem solving, working memory, and motor correlates of association and commissural fiber bundles in normal aging: A quantitative fiber tracking study. *Neuroimage*, *44*, 1050–1062.